

A population of isolated hard X-ray sources near the supernova remnant Kes 69

F. Bocchino¹, A.M. Bykov², Y. Chen^{3,4}, A.M. Krassilchtchikov^{2,5}, K.P. Levenfish², M. Miceli^{6,1},
G.G. Pavlov^{7,5}, Yu.A. Uvarov^{2,5}, X. Zhou⁸

¹ INAF-Osservatorio Astronomico di Palermo, Piazza del Parlamento 1, 90134 Palermo, Italy; bocchino@astropa.unipa.it

² A.F. Ioffe Institute for Physics and Technology, St. Petersburg, Russia, 194021; byk@astro.ioffe.ru

³ Department of Astronomy, Nanjing University, Nanjing, 210093, China

⁴ Key Laboratory of Modern Astronomy and Astrophysics (Nanjing University), Ministry of Education, China

⁵ St. Petersburg State Polytechnical University, St. Petersburg, Russia, 195251

⁶ Dipartimento di Fisica, Università di Palermo, Piazza del Parlamento 1, 90134 Palermo, Italy

⁷ 525 Davey Laboratory, Pennsylvania State University, University Park, PA 16802; pavlov@astro.psu.edu

⁸ Purple Mountain Observatory, CAS, 2 West Beijing Road, Nanjing 210008, China

Preprint online version: November 16, 2018

ABSTRACT

Recent X-ray observations of the supernova remnant IC443 interacting with molecular clouds have shown the presence of a new population of hard X-ray sources related to the remnant itself, which has been interpreted in terms of fast ejecta fragment propagating inside the dense environment. Prompted by these studies, we have obtained a deep *XMM-Newton* observation of the supernova remnant (SNR) Kes 69, which also shows signs of shock-cloud interaction. We report on the detection of 18 hard X-ray sources in the field of Kes 69, a significant excess of the expected galactic source population in the field, spatially correlated with CO emission from the cloud in the remnant environment. The spectra of 3 of the 18 sources can be described as hard power laws with photon index < 2 plus line emission associated to K-shell transitions. We discuss the two most promising scenarios for the interpretation of the sources, namely fast ejecta fragments (as in IC443) and cataclysmic variables. While most of the observational evidences are consistent with the former interpretation, we cannot rule out the latter.

Key words. ISM: individual (Kes 69) — supernova remnants — X-rays: ISM

1. Introduction

The high-resolution X-ray imaging of supernova remnants (SNRs) interacting with dense ambient matter has shown that a population of previously unknown compact sources are sometimes present in the field of view, visible at high X-ray energies (above ~ 2 keV). These are the X-ray shrapnels – the ballistically moving isolated fragments of ejected material radiating both thermal and non-thermal X-rays (Bykov et al. 2005, 2008).

Ejecta fragments have been long known (Aschenbach et al. 1995; Miyata et al. 2001; Laming & Hwang 2003), but when they reach a dense cloud, they may become bright and compact sources in IR (Bykov et al. 2008) and X-ray, with luminosity $L_X > 10^{31}$ erg s⁻¹ (Bykov 2002, 2003). Since the fragment lifetime in the cloud is about a few hundred years, a few of such isolated sources are expected to be visible in the field of an SNR entering a molecular cloud. The shrapnel-type sources produce multicomponent X-ray spectra consisting of: (i) a relatively faint thermal continuum with $kT \lesssim 1$ keV, (ii) a power-law nonthermal continuum with photon index ~ 1.5 , and (iii) non-thermal line emission due to K-shell ionization produced by the intense flux of electrons (accelerated at the bow-shock) that collide with a metal-rich ejecta fragment.

The ballistically moving clumps are potentially an important source of information about the explosive supernova (SN) event. In fact, they presumably correspond to initial ejecta inhomogeneities, located in the faster outer layers, and their chemical composition may be indicative of the nucleosynthesis processes which occurred at early stages of SN evolution. Therefore, they provide complementary information with respect to the rest of X-ray emitting ejecta. It should be noted, however, that a firm detection of an ejecta fragment is a challenging task, because fragment's lifetime is only a few hundred years, and the brighter is the fragment, the shorter is the lifetime.

SNRs interacting with molecular clouds are the natural sites to study the physics of fast fragments. One of the best cases is IC 443, which emits bright molecular lines of OH, CO, and H₂, excited by a shock. IC 443 is an extended object (about 45' in size at a distance of about 1.5 kpc) with the brightest GeV gamma-ray emitting SNR shell (Abdo et al. 2010). It is also a source of TeV gamma-rays (Albert et al. 2007). Hard X-ray sources in IC 443 related to shocked clumps have been detected by Bocchino & Bykov (2000) and further studied by Bocchino & Bykov (2003), Bykov et al. (2005), Bocchino et al. (2008) and Bykov et al. (2008).

Motivated by the results obtained in the SNR IC 443, we have started an observational campaign aimed at de-

tection of fast fragments in SNRs interacting with molecular clouds. The SNR G21.8–0.6 (Kes 69) is a good candidate where such sources may be seen. It is an extended incomplete radio shell of about $20'$ in size (e.g., Shaver & Goss 1970) at an estimated distance of about 5.2 kpc (e.g., Tian & Leahy 2008; Zhou et al. 2009). The Imaging Proportional Counter aboard the *Einstein Observatory* was used by Seward (1990) to obtain a noisy X-ray image of Kes 69. Using *ROSAT* PSPC observations, Yusef-Zadeh et al. (2003) estimated an absorbing column of $N_{\text{H}} = 2.4 \times 10^{22} \text{ cm}^{-2}$.

Spitzer observations of Kes 69 by Reach et al. (2006) and Hewitt et al. (2009) have revealed bright molecular emission lines of OH, CO, and H_2 , excited by a shock. In particular, the SNR contains a filament along the bright southern radio shell of $\sim 15'$ extension seen with *Spitzer* IRAC in the $4.5 \mu\text{m}$ band and attributed to the molecular hydrogen emission line, as well as an extended OH (1720 MHz) emission region that indicates the presence of a molecular shock (see Hewitt et al. 2009, and references therein). Millimeter band observations of CO and HCO^+ lines towards Kes 69 performed by Zhou et al. (2009) provided strong evidence for the association between Kes 69 and the $\sim +85 \text{ km s}^{-1}$ component of molecular gas.

The established interaction of Kes 69 with a molecular cloud makes this SNR a promising target for a search of shrapnel X-ray sources. Since the size of the remnant (about $20'$) is comparable with the field of view of *XMM-Newton* EPIC cameras, we conducted *XMM-Newton* observations of the field to study the faint population of hard compact X-ray sources and look for the signature of fast ejecta fragments. Here we report the detection of 18 sources in the field of Kes 69, a significant excess with respect to the expected Galactic field sources of the same flux. We have found some of these sources to emit hard power law spectra with possible $\text{K}\alpha$ X-ray lines of Si, Fe, Ca, and Ti. Such spectra support the suggested shrapnel nature of the sources.

2. *XMM-Newton* observations and data analysis

The field of Kes 69 was observed with the *XMM-Newton* observatory (Jansen et al. 2001) on 2009 October 8 (ObsID 0605480101, PI: M. Miceli) for 60 ksec with the EPIC-MOS camera (Turner et al. 2001) in the Full Frame Mode and with the EPIC-PN camera (Strüder et al. 2001) in the Extended Full Frame Mode (the medium filter was used for all the cameras). In the course of *XMM-Newton* data reduction, we selected EPIC events with FLAG=0, patterns 0–4 for EPIC-PN camera, and patterns 0–12 for EPIC-MOS cameras.

To filter out periods of enhanced particle background, the original event lists were screened by using the sigma-clipping algorithm of the ESAS software¹. After the filtering, the net good time exposure of the field was reduced to about 54 ks. SAS v9.0.0 was used for EPIC data processing, and the HEASOFT 6.3 suite, including XSPEC v.12.3.1, was used for spectral fitting.

3. Results

3.1. Diffuse emission

Hard (3–10 keV) and soft (1–3 keV) X-ray maps of Kes 69 are shown in Figure 1. Diffuse X-ray emission is clearly seen on the latter map. The diffuse emission region is bordered by the radio emission contours obtained from the 1.4 GHz NVSS survey (Condon et al. 1998). No significant diffuse emission is found on the hard X-ray map, while several point-like sources are present. We verified that the brightest fluctuation of the residual diffuse emission in the hard X-ray map is at the level of only 3σ above the background. The faint fluctuations generally correlates with the bright soft X-ray emission, so we argue that the very faint hard diffuse emission is the tail of the thermal emission visible in the soft X-ray map, and we do not consider it any further.

Spectral analysis of the diffuse extended emission of a mixed morphology SNR requires a thorough modeling of multiple components, both thermal (with possibly overionized plasma) and nonthermal. Such a detailed analysis of the diffuse soft X-ray emission of Kes 69 is beyond the scope of this work. However, to estimate the absorption column toward this remnant and to compare it to the absorption of the compact sources, a spectrum of the extended diffuse emission region in the southern shell (shown as black rectangle in the middle panel of Figure 1) has been extracted and fitted with the absorbed thermal plasma *mekal* model. For the spectral fitting, a channel binning with at least 15 counts per bin was used. The fitting yielded $N_{\text{H}} = (2.8 \pm 0.4) \times 10^{22} \text{ cm}^{-2}$, $T = (0.8 \pm 0.2) \text{ keV}$ (errors are at the 99% confidence level). The absorption column depth is consistent with that derived previously from the *Einstein* and *ROSAT* observations. The higher temperature in the *ROSAT* fit derived by Yusef-Zadeh et al. (2003) is most likely due to the contribution of the point sources unresolved by *ROSAT* in the wide region analyzed. The post-shock temperature $T \approx 0.8 \text{ keV}$ corresponds to the estimated age of about 10,000 years, assuming the Sedov stage solution. The forward shock velocity can be estimated as $\sim 1,000 \text{ km s}^{-1}$. The velocities of the isolated ejecta fragments in the vicinity of the shell should be comparable to the shock velocity.

3.2. Hard X-ray sources detection and spectroscopy

The SAS task edetect_chain was applied to the 3–10 keV image to detect and study the population of point-like sources in the field of Kes 69 and to identify the sources likely associated with this remnant. The thermal emission from the SNR makes almost no contribution in the energy band chosen. Eighteen sources, whose properties are listed in Table 1, have been detected with the likelihood above 30σ (marked in Figure 1). The positions of the hard X-ray sources are remarkably correlated with the ^{12}CO emission at the velocity associated with the SNR ($80 - 81 \text{ km s}^{-1}$, Zhou et al. 2009), whose image and contours are shown in Figure 1. The correlation is better seen in Figure 2, which shows that the average brightness CO temperature at the location of the 18 sources is higher than the average cloud brightness temperature, which means that the hard X-ray sources tend to be preferentially found in dense regions indicated by bright CO emission (see Appendix A for details

¹ <http://xmm.esac.esa.int/pub/xmm-esas/xmm-esas.pdf>

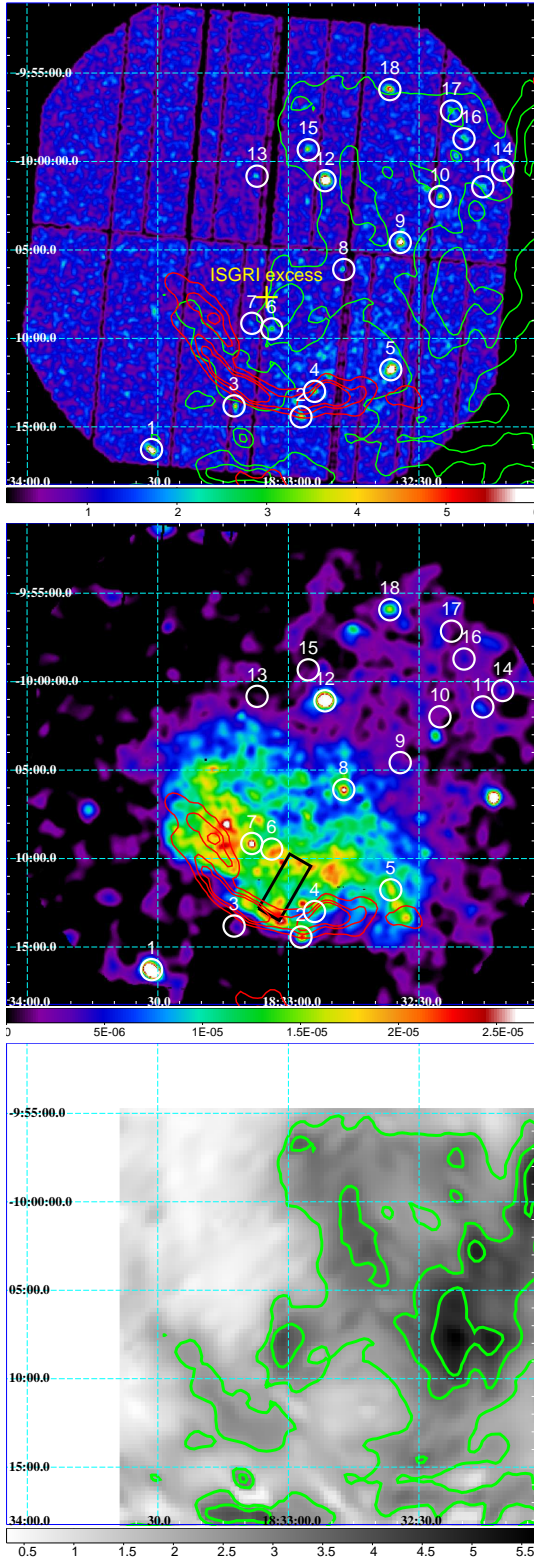


Fig. 1. *Upper panel:* EPIC PN count map of Kes 69 obtained in the 3–10 keV band. The bin size is $4''$. The white circles indicate point-like sources detected in this image; the red contours denote intensity of the 1.4 GHz emission from the NVSS survey (Condon et al. 1998); the green contours denote the ^{12}CO ($J = 1 - 0$) intensity in the 80–81 km s^{-1} velocity range (see lower panel). The yellow cross denotes the position of the hard X-ray excess seen with *INTEGRAL* ISGRI. *Middle panel:* Adaptively smoothed (to a signal-to-noise ratio of 16) and vignetting-corrected EPIC count-rate image (MOS-equivalent counts per second per bin) of Kes 69 in the 1–3 keV band. The black rectangle is the region used for the spectrum of the diffuse emission. The superimposed hard X-ray sources and the radio contours are the same as in the upper panel. *Lower panel:* ^{12}CO ($J = 1 - 0$) intensity map in the velocity interval 80–81 km/s (linearly interpolated to a resolution of $0''.24$ (see Zhou et al. 2009)). The contour levels are at 40%.

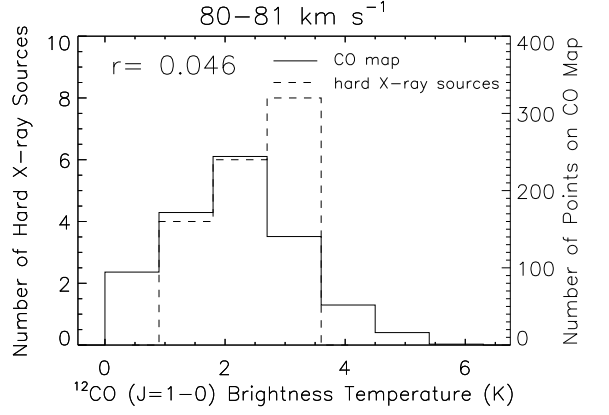


Fig. 2. Histogram of brightness temperature values in the ^{12}CO maps in the 80–81 km s^{-1} velocity range (Zhou et al. 2009, also visible in the lower panel of Fig. 1) which shows the molecular cloud interacting with the remnant (solid line). Overimposed, the histogram of the same temperatures at the location of the 18 hard X-ray sources detected in the *XMM-Newton* observation (dashed line). The r value is the Pearson correlation coefficient, indicating a positive correlation (see appendix A for details). The source peak is offset toward higher value with respect to the cloud mean value, indicating that X-ray sources cluster at brighter-than-average CO map points.

about this method). The general correlation between the source position and the molecular cloud that is interacting with the remnant makes the sources good candidates for X-ray emitting ejecta fragments.

We have extracted the EPIC spectra for all the sources rebinned to achieve a signal-to-noise ratio > 4 per bin, and fitted simultaneously both MOS and PN spectra. The ancillary response files were produced with the SAS ARFGEN task, and the EVIGWEIGHT task (Arnaud et al. 2001) was used to correct for vignetting effects. An empty area in the northeastern part of the image was used as a background region. Parameters of power law fits to the spectra of the point-like hard sources are listed in Table 1.

Src 3, 5 and 18 were selected for a detailed study based on the possible presence of X-ray line emission lines in the spectrum similar to those expected in fast moving ejecta knot according to Bykov (2002). The lines in Src 3 and 5 can be interpreted as Fe line complex and as traces of the 1.8 keV Si line. The observed line features at 3.5 keV and 4.7 keV in Src 13 could originate from ^{40}Ca and ^{48}Ti , respectively.

The spatial count distributions of Src 3, 5, and 13 are consistent with that of a point source. It should be noted here that with the few arcsec resolution of *XMM-Newton* the upper limit of a point-like source extension at the estimated distance of 5.2 kpc is about 10^{17} cm.

Two circular regions of $16''$ radius centered at Src 3 and Src 5 were chosen for spectral analysis. Unfortunately, both sources were projected onto the damaged MOS1 CCD6 chip; therefore only PN and MOS2 events were taken into account. For spectral analysis of Src 13 a circular region of $20''$ radius containing 160 PN counts was chosen. A 10

Table 1. List of sources detected in the 3–10 keV band in the field of view of the XMM-Newton observation of the Kes 69 SNR

Src	Name	Count-rate PN cnt ks ⁻¹	N_H 10 ²² cm ⁻²	Γ	χ^2/dof	$10^{-14}F_{2-10\text{ keV}}$ erg cm ⁻² s ⁻¹	Possible association in SIMBAD within 15''
1	XMMU J183331.4-101616	9.8 ± 2.0	0.7 ^{+0.3} _{-0.2}	1.2 ^{+0.2} _{-0.2}	1.1	23 ⁺⁴ ₋₁₂	
2	XMMU J183257.1-101426	8.1 ± 0.8	2.6 ^{+1.6} _{-1.0}	2.3 ^{+0.9} _{-0.5}	0.82	4.4 ^{+1.4} _{-3.3}	IRAS 18302-1016 (13'')
3	XMMU J183312.4-101349	10.6 ± 0.9	3.6 ^{+2.1} _{-1.1}	0.6 ^{+2.8} _{-2.8}	0.47	2.5 ^{+1.3} _{-1.3}	1XMM J183312.5-101351 (1'')
4	XMMU J183254.0-101259	4.2 ± 0.6	1.7 ^{+1.9} _{-0.9}	1.7 ^{+1.0} _{-0.8}	0.82	2.9 ^{+1.1} _{-2.2}	
5	XMMU J183236.4-101146	35.3 ± 2.3	3.0 ^{+1.0} _{-1.0}	0.6 ^{+0.3} _{-0.2}	1.1	16 ⁺⁴ ₋₁₅	XGPS-I J183236-101144 (3'')
6	XMMU J183303.8-100928	4.0 ± 0.5	1.2 ^{+1.9} _{-1.0}	1.0 ^{+1.2} _{-0.9}	1.2	2.2 ^{+0.9} _{-1.5}	
7	XMMU J183308.4-100909	3.2 ± 0.5	0.5 ^{+0.5} _{-0.3}	1.7 ^{+0.8} _{-0.7}	0.84	1.1 ^{+0.6} _{-0.8}	
8	XMMU J183247.2-100606	4.3 ± 0.6	0.6 ^{+0.6} _{-0.2}	1.6 ^{+0.8} _{-0.7}	1.2	1.8 ^{+0.6} _{-1.3}	
9	XMMU J183234.3-100434	10.9 ± 1.1	45 ⁺³³ ₋₂₅	4.0 ^{+3.0} _{-3.0}	1.1	5.7 ^{+1.3} _{-5.7}	2MASS J18323431-1004360 (1'') ^a
10	XMMU J183225.2-100159	6.2 ± 0.7	21 ⁺⁴² ₋₁₈	2.8 ^{+5.9} _{-3.1}	0.86	3.4 ^{+0.9} _{-3.39}	XGPS-I J183225-100158 (0.5'')
11	XMMU J183215.3-100125	5.7 ± 0.8	< 3.5	1.1 ^{+2.6} _{-1.5}	0.57	2.6 ^{+1.9} _{-2.5}	
12	XMMU J183251.6-100105	5.8 ± 1.4	0.7 ^{+0.1} _{-0.1}	1.25 ^{+0.1} _{-0.1}	0.97	26 ⁺³ ₋₅	XGPS-I J183251-100106 (1'') ^b
13	XMMU J183307.2-100050	3.0 ± 0.5	0.8 ^{+1.7} _{-0.5}	1.1 ^{+4.8} _{-0.9}	0.42	1.4 ^{+1.0} _{-0.8}	
14	XMMU J183210.8-100029	9.2 ± 1.1	< 9.0	0.2 ^{+3.1} _{-0.8} ^c	1.35	3.3 ^{+1.7} _{-2.7}	XGPS-I J183210-100031 (1'')
15	XMMU J183255.4-095920	6.3 ± 0.7	11 ⁺²¹ ₋₉	1.2 ^{+2.8} _{-1.9}	1.4	4.2 ^{+1.4} _{-4.1}	
16	XMMU J183219.6-095843	8.0 ± 1.0	8.4 ^{+14.6} _{-6.2}	2.5 ^{+3.1} _{-2.1}	0.79	3.2 ^{+1.1} _{-3.0}	
17	XMMU J183222.5-095708	9.0 ± 1.0	15 ⁺³⁷ ₋₁₁	1.6 ^{+4.9} _{-1.8}	1.1	4.7 ^{+1.4} _{-4.7}	
18	XMMU J183236.7-095556	20.0 ± 1.4	< 0.7	0.2 ^{+0.4} _{-0.5}	1.0	11 ^{+3.5} _{-6.5}	

^a $m_J = 16.1$.

^b An $m_R=21.6$ star, according to Motch et al. (2010).

^c 1 σ errors.

counts per bin PN spectrum was used to locate the positions of line features in the spectrum.

3.2.1. Src 5

Src 5 was first detected by Hands et al. (2004) in the *XMM-Newton* Galactic Plane Survey (XGPS). This source is brighter than Src 3 and Src 13, and its spectrum is shown in the upper panel of Figure 3. A simple absorbed power-law model provides $\chi^2 = 63.9$ (at 46 dof), but it does not fit the bright line-like features visible at about 1.8 keV and 6.5 keV. The quality of the fit improves significantly by adding two narrow gaussians to describe the lines². We found that the line energies are 1.84^{+0.06}_{-0.06} keV and 6.64^{+0.06}_{-0.08} keV, respectively, the photon index is $\Gamma = 0.6$ ^{+0.3}_{-0.2}, and the improved χ^2 is 47.8 (at 43 dof). Confidence contours for the line normalization coefficients and line energies are shown in the upper panels of Figure 4. The line features can be associated with K-shell transitions of Si (at 1.85 keV) and Fe (at 6.64 keV) originating from a metal-rich ejecta knot. Assuming that the source is at the same distance of 5.2 kpc as Kes 69, the line luminosities are $\sim 6 \times 10^{39}$ photons s⁻¹ for the Si line, and $\sim 3 \times 10^{39}$ photons s⁻¹ for the Fe line (with relatively large uncertainties, as shown in Figure 4, upper panels). Both these values and the ratio of the Si and Fe line luminosities are in agreement with those predicted for fast (~ 2700 km s⁻¹) and small (size of 3×10^{16} cm) ejecta knots having a mass of $10^{-3} M_\odot$ moving inside a dense ($\sim 10^3$ cm⁻³) molecular cloud (see Table 1 in Bykov 2002, where luminosities for a fragment are shown).

² Since the absorbing column $N_H=3.8$ ^{+1.2}_{-1.5} $\times 10^{22}$ cm⁻² is consistent with that found for the whole remnant, we fixed it here to 4×10^{22} cm⁻² to obtain more restricted estimations of the other model parameters.

We investigate a possible thermal origin of Src 5 by fitting its spectrum with an absorbed thermal model. Although the probable Si line is not well described by this model, the quality of the fit is still acceptable ($\chi^2 = 52.3$ at 46 dof). The best-fit parameter values for the thermal fit are $kT = 8.8$ ^{+3.7}_{-2.1} keV and $N_H = (7.8$ ^{+2.4}_{-1.6}) $\times 10^{22}$ cm⁻². Since in the thermal scenario the column density is higher than that found for Kes 69, a lower limit for the distance to Src 5 is 5.2 kpc (i.e. the distance to the remnant), and its X-ray luminosity is $> 10^{33}$ erg/s. These extreme values can be indicative of a very energetic coronal flare, as X-ray luminosities up to $\sim 10^{33}$ erg s⁻¹ and temperatures up to 10 keV have been observed in the most energetic flares of active stars (e.g., Favata et al. 2005). Another possible source of such a high temperature and luminosity could be a cataclysmic variable star (CV). Nevertheless, we point out that by comparing the source count-rate in our observation with that observed by Hands et al. (2004) in the XGPS observations (17.1 \pm 0.7 PN counts/ks and 19.3 \pm 3.8 PN counts/ks, for Src 3 and Src 5, respectively, in the 0.4–6 keV band), we found that the source luminosity is consistent with being constant. Also, the hardness ratio of 0.75 obtained by Hands et al. (2004) is very similar to 0.70 \pm 0.05 obtained in our new observation. The stationarity of the X-ray luminosity and hardness ratio both concur in making a coronal flaring or a CV origin of Src 5 unlikely, though still not excluded (see also Section 5).

3.2.2. Src 3

The background-subtracted spectrum of Src 3 is shown in the middle panel of Figure 3. This spectrum is substantially absorbed (model N_H values are about 10^{22} cm⁻² – consistent with that of the soft diffuse emission from the

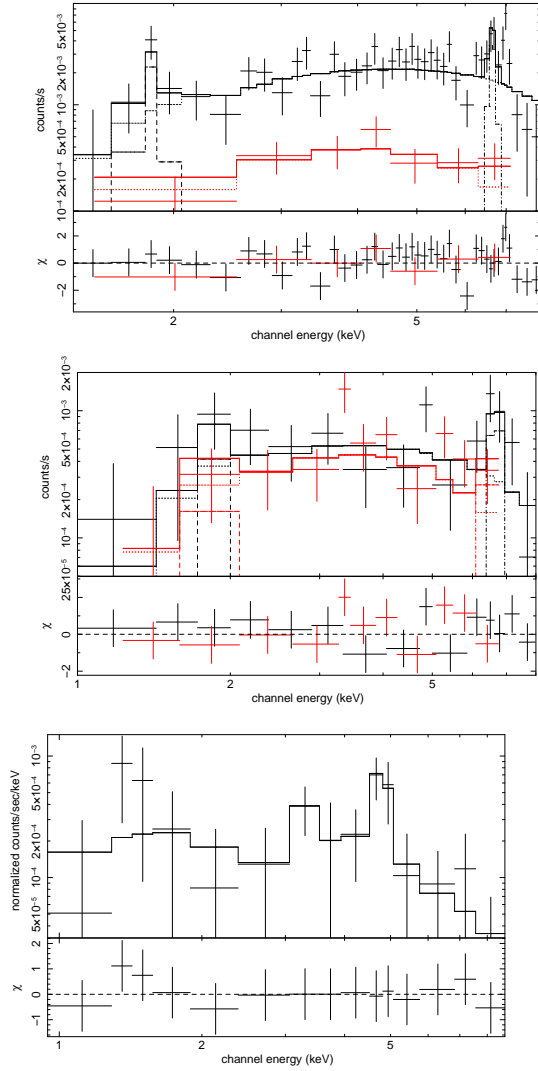


Fig. 3. *XMM-Newton* EPIC-PN (black) and MOS2 (red) spectra of Src 5 (*upper panel*), Src 3 (*middle panel*), and Src 13 (*lower panel*) with best-fit models (power law plus two narrow gaussians) and residuals.

remnant), and contains line-like features at about 1.8 keV and 6.7 keV. Like in Src 5, we fixed the N_{H} to $4 \times 10^{22} \text{ cm}^{-2}$, and found that a power law model with $\Gamma = 1.3_{-0.7}^{+0.5}$ and two narrow gaussians³ describes the spectra significantly better than a simple power law model ($\chi^2=20.4$ at 21 dof, and $\chi^2=28.5$ at 22 dof, respectively). Assuming that Src 3 is at 5.2 kpc, the Fe line luminosity is $(1.6 \pm 0.9) \times 10^{39}$ photons s^{-1} and the Si line luminosity is $< 6 \times 10^{39}$ photons s^{-1} . The best-fit values are in good agreement with those predicted by Bykov (2002) for a supersonic ejecta fragment propagating in a molecular cloud, the only difference from Src 5 being a smaller best-fit velocity ($\sim 1000 \text{ km s}^{-1}$). We investigated a possible thermal origin of Src 3 by fitting its spectrum with an absorbed thermal model and found that, with such a model, we can only constrain the temperature to be above 7 keV.

³ Because of the poorer statistics, we fixed the line energies to those found for Src 5.

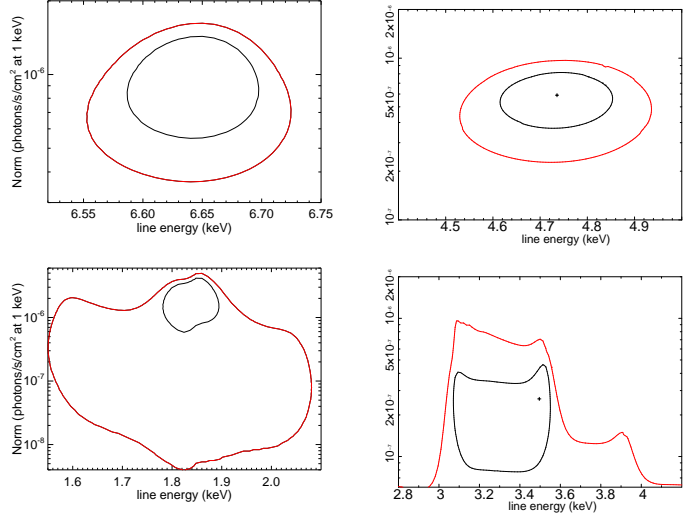


Fig. 4. Confidence contours of the line centroid and normalization for the Fe (*upper left*) and Si (*lower left*) lines in Src 5, and for the ^{48}Ti (*upper right*) and Ca (*lower right*) lines in Src 13. The contours correspond to the 68% and 90% confidence levels.

3.2.3. Src 13

A background-subtracted spectrum of Src 13 is shown in the lower panel of Figure 3. The spectrum contains line-like features at about 3.5 keV and 4.7 keV. Confidence contours for the line normalization coefficients and line energies are shown in the lower panels of Figure 4. A power law model with $\Gamma = 1.1_{-0.9}^{+4.8}$ and two narrow gaussians at fixed energies fits the spectrum ($\chi^2=11.0$ at 31 dof). The line luminosities at 5.2 kpc are about 7.3×10^{38} photons s^{-1} and 1.7×10^{39} photons s^{-1} for the 3.5 keV and 4.7 keV lines, respectively, in agreement with the range of values predicted for an ejecta fragment in a molecular cloud. Unlike the spectra of Src 3 and 5, the spectrum of Src 13 does not show Fe complex line features, a fit with a thermal model is much worse than the non-thermal one.

4. Hard X-ray *INTEGRAL* ISGRI Data of Kes 69

The field of Kes 69 was a target of Galactic plane scans with the *INTEGRAL* gamma-ray observatory. The archival data obtained with the ISGRI camera during the scans comprise about 1700 ks of fully coded field of view observations in the years 2002 – 2010.

A weak hard X-ray source is marginally seen in the central part of the remnant (see the upper panel of Figure 1). The source position is close to the projected center of an imaginary triangle with vertices in Src 3, 5, and 13. The HEAVENS⁴ survey (Walter et al. 2010) provides 3σ detections in the 18 – 50 keV and 50 – 150 keV bands (see the lower right panel of Figure 3). To estimate the hard X-ray flux of the sources, intercalibration with a bright nearby SNR G21.5–0.9 (e.g., Krivonos et al. 2007) was performed to yield $5.7 \times 10^{-12} \text{ erg cm}^{-2} \text{ s}^{-1}$ in the 18 – 60 keV band, and $1.2 \times 10^{-12} \text{ erg cm}^{-2} \text{ s}^{-1}$ in the 60 – 120 keV band.

The highest plasma temperatures consistent with the *XMM-Newton* data, discussed in §3, are too low to yield

⁴ <http://www.isdc.unige.ch/heavens/>

Table 2. Fluxes of possible infrared counterparts to Src 3, 5, and 13. Infrared fluxes of Src *o51*, *o31*, *o32*, *o13* are quoted for *Spitzer* IRAC bands I1, I2, I3, I4, *Spitzer* MIPS band M1, and 2MASS bands J, H, K_s (see Figure 5). The flux units are 10^{-13} erg cm^{-2} s^{-1} . Errors are at the 68% level. Estimates of extinction factors (i.e. the value $10^{A_{\text{band}}/2.5}$, A_V is computed from the X-ray absorption) at positions of Src 3 and 5 are listed as *ext5* and *ext3*.

Band	I1	I2	I3	I4	M1	J	H	K_s
λ , μm	3.6	4.5	5.8	8.0	24	1.2	1.7	2.2
Source								
<i>o51</i>	2.2 \pm 0.1	1.5 \pm 0.1	<1.6	<1.6	<0.9
<i>o31</i>	4.5 \pm 0.1	2.4 \pm 0.1	<1.2	<1.4	<2.7	...	3.8 \pm 0.4	4.5 \pm 0.3
<i>o32</i>	210 \pm 0.9	120 \pm 0.4	91.0 \pm 0.8	54.1 \pm 0.4	6.3 \pm 0.1	6.3 \pm 0.2	75 \pm 1.6	140 \pm 2.7
<i>o13</i>	5.4 \pm 0.4	2.9 \pm 0.3	2.0 \pm 0.3	1.5 \pm 0.3	...	2.2 \pm 0.2	6.6 \pm 0.2	<5.9
<i>ext5</i>	4.0	3.5	3.2	2.8	1.0	575	58	13
<i>ext3</i>	2.5	2.4	2.2	2.0	1.0	76	16	5.8

ISGRI detection above 60 keV. Thus, the detection of the INTEGRAL source associated with Kes 69 is evidence in favor of a non-thermal origin of the emission from (at least some of) the compact sources of this remnant. The power-law models for Src 3, 5, and 13 obtained from the *XMM-Newton* data would yield $(1-5) \times 10^{-12}$ erg cm^{-2} s^{-1} in the 18–60 keV band, which is compatible with the flux detected by ISGRI in the same band. The extrapolation of the power-law model of the three sources to the 60–120 keV band would yield a flux higher than the flux observed by ISGRI in that band. Therefore, if the sources were indeed the X-ray counterpart of the ISGRI emission, a spectral break would be required around 60 keV.

5. IR imaging and photometry of Kes 69

The field of Kes 69 was the target of *Spitzer* MIPS observations r15602176, r15584768, r15621120, r15634432, and r15627008, performed on 2005 Sep 30 (PI: S. Carey) and *Spitzer* IRAC observations r12103680, r12107264, and r12110592, performed on 2004 Oct 07 (PI: E. Churchwell).

The standard MOPEX 18.4.9 software (Makovoz et al. 2006) was used to construct mosaic images and detect point sources from the archival BCD-level data pre-processed by the S18.7.0 (IRAC) and S18.12.0 (MIPS) pipelines. The net exposure of the mosaic maps was equal to 2–5 frames of 1.2 s (IRAC) and 10–18 frames of 2.62 s (MIPS).

Two point-like sources were found in the immediate vicinity of Src 3 (see the upper panels of Figure 5) at $\alpha = 18^{\text{h}}33^{\text{m}}12^{\text{s}}.0$, $\delta = -10^{\circ}13'49''$ (source *o31*, 6.2'' from the X-ray source) and at $\alpha = 18^{\text{h}}33^{\text{m}}12^{\text{s}}.6$, $\delta = -10^{\circ}13'53''$ (source *o32*, at 4.7''). Two point-like sources were found in the immediate vicinity of Src 5 (see the lower panel of Figure 5) at $\alpha = 18^{\text{h}}32^{\text{m}}32^{\text{s}}.2$, $\delta = -10^{\circ}11'45''$ (source *o51*, at < 1'' from the X-ray source) and at $\alpha = 18^{\text{h}}32^{\text{m}}36^{\text{s}}.5$, $\delta = -10^{\circ}11'46''$ (source *o52*, at 4.3''). All these positions are in the J2000 reference frame. Another point-like source is clearly seen at about 2'' from Src 13 (see Figure 6) at $\alpha = 18^{\text{h}}33^{\text{m}}07^{\text{s}}.2$, $\delta = -10^{\circ}00'48''$ (source *o13*).

The source *o52*, listed in the USNO-B1.0 catalogue (Monet et al. 2003), has $B = 17.7$, $R = 14.1$, which means that it is most likely a foreground star. The other four sources can be treated as the possible infrared counterparts of Src 3, 5, and 13. Medium IR fluxes of these sources measured with MOPEX and near IR fluxes listed in the 2MASS survey (Skrutskie et al. 2006) are summarized in Table 2 along with extinction factors.

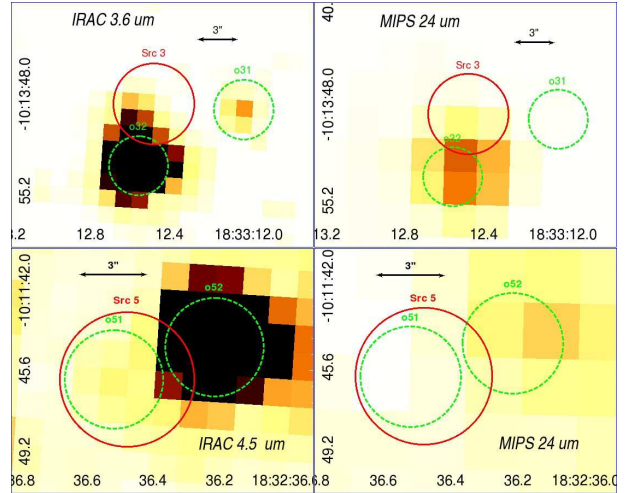


Fig. 5. Environments of Src 3 (*top panels*) and Src 5 (*bottom panels*) as seen by *Spitzer* IRAC camera at 3.6 and 4.5 μm , and MIPS at 24 μm . The sources Src 3 and Src 5 detected by *XMM-Newton* are shown as solid red circles, while the IR sources are shown as dashed green circles, both with labels with names referred to in the text.

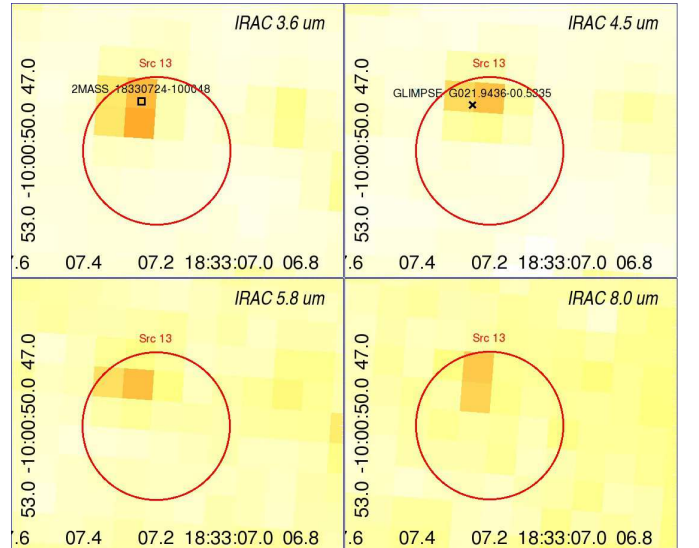


Fig. 6. Close environments of Src 13 as seen with *Spitzer* IRAC at 3.6, 4.5, 5.8 and 8.0 μm . The red circle marks the position of the *XMM-Newton* detected source.

As no specific data can be found in the available catalogs to estimate the distances and velocities or somehow indicate the nature of the IR sources that are possibly connected with Src 3, 5, and 13, it is useful to compare the IR colors of Src *o51*, *o31*, *o32*, and *o13* with those typical for various classes of objects, paying a particular attention to ejecta fragment candidates and CVs, which have been pointed out as plausible interpretations of Src 3, 5 and 13.

The F_{11}/F_{13} and F_{12}/F_{14} flux ratios of Src *o51*, *o31*, *o32*, and *o13* are larger than those in Figure 2 of Reach et al. (2006), which contains examples of IRAC flux ratios of shock-excited zones in SNRs. The $m_{11}-m_{12}$ and $m_{12}-m_{13}$ colors of Src *o51*, *o31*, *o32*, *o13* are well within the range of IRAC colors reported by Stolovy et al. (2006) and Gezari et al. (2006) for faint X-ray sources in the Galactic Center region, which are usually interpreted as accreting binaries. The IR spectral energy distribution of a CV source AE Aqr reported by Dubus et al. (2007) is similar to that of Src *o32*, but $24\mu\text{m}$ flux of Src *o32* rescaled to the distance of AE Aqr (102 pc) appears much lower. Thus, the assumption that the potential IR counterparts of Src 3 and 5 are CVs seems unlikely, although there is also no firm evidence for detection of an ejecta fragment in the IR bands. However, it should be noted that the $\sim 10^{34}$ erg s^{-1} IR luminosities of the possible counterparts of Src 3, 5, and 13 are within the range predicted for IR emission of ejecta fragments interacting with molecular clouds (see e.g. Bykov et al. 2008).

6. Discussion

6.1. Interpretation as ejecta fragments

The apparent correlation of the location of the hard X-ray sources detected in the field of Kes 69 with the CO emission of molecular material associated with the remnant together with consistent values of absorbing columns obtained from X-ray spectra of the sources naturally leads to an SNR-related interpretation. Moreover, there is an apparent excess of the sources with 2–10 keV fluxes above $(2-3) \times 10^{-14}$ erg cm^{-2} s^{-1} within the region of about $15' \times 20'$ size where the SNR is interacting with the molecular cloud (shown in Figure 1). The $\log(N) - \log(S)$ statistics of X-ray sources in the *XMM-Newton* Galactic plane survey by Motch et al. (2010) predicts about 40 sources of 2–10 keV flux above 3×10^{-14} erg cm^{-2} s^{-1} per square degree. Therefore, only about 3–4 galactic field sources are expected in the region on the statistical ground. The X-ray luminosities of the sources are $L_X \gtrsim 10^{31}$ erg s^{-1} if they are located at the estimated distance of Kes 69.

If the source are related to Kes 69, then isolated “shrapnels” or “knots”, associated with fast moving ejecta fragments, form an interesting explanation for a population of hard X-ray sources in the field of SNRs. A massive individual fragment moving supersonically through a molecular cloud would have a luminosity $L_X \gtrsim 10^{31}$ erg s^{-1} in the 1–10 keV band and would be observable with *XMM-Newton* and *Chandra* from a few kpc distance. Such fragments have indeed been detected in hard X-rays inside the IC 443 SNR (Bocchino et al. 2008, Bykov et al. 2008, and references therein), and the X-ray sources in Kes 69, which is also interacting with molecular material (Zhou et al. 2009), can also be interpreted in the same way.

The model of fast supernova fragments predicts two X-ray emission components (Bykov 2003). The first one is

thermal X-ray emission from a hot shocked ambient gas behind the fragment bow shock, with the spectrum of an optically thin thermal shocked plasma of an ISM cloud abundance. The second emission component is nonthermal. Interaction of the fast electrons (accelerated at the fragment bow-shock) with the fragment body produces both hard continuum and X-ray and IR line emission, including the K-shell lines of the Si and Fe group elements (Bykov 2002)⁵.

As mentioned in Sect. 3.2, the upper limit of a point-like source extension at the estimated distance of 5.2 kpc is about 10^{17} cm. Individual compact fragments of scale sizes below $\sim 10^{17}$ cm would be optically thick to the K-shell X-ray line absorption if the metal content in the source exceeds about $10^{-4} M_\odot$. Indeed, for Li-like to F-like ions the probability of auto-ionization by a K_α photon (i.e., the resonant Auger destruction) is significantly larger than that of photon re-emission (see, e.g., Liedahl 2005), resulting in the true line photon absorption. The line optical depth τ_X with respect to the resonant absorption of a K_α line of energy E_X (in keV) for an element X (of atomic weight A) can be estimated as

$$\tau_X \simeq 3 \cdot \frac{f_{lu}}{0.5} \cdot \frac{\xi_{X^i}}{0.4} \cdot A^{0.5} \cdot N_{X,17} [T_6 + A \cdot (2.3 \times 10^3 \beta_{\sigma_v})^2]^{-0.5} E_X^{-1}, \quad (1)$$

where ξ_{X^i} is the relative abundance of the ion i of the element X , $N_{X,17}$ is the column density of the element X in the source along the line of sight in units of 10^{17} cm^{-2} , and f_{lu} is the relative line oscillator strength of the K_α line. The characteristic line width is assumed to be equal to the Doppler full width at half maximum, in which both the thermal ion velocity for temperature $T = 10^6 \cdot T_6$ K and the micro-turbulent velocity ($\beta_{\sigma_v} = \sigma_v/c$) are accounted for (see, e.g., Nicastro et al. 1999).

This implies, in particular, that the line fluxes of such fragments are expected to be about 10^{31} erg s^{-1} for most of the X-ray lines, and that, for example, ^{40}Ca and ^{48}Ti line fluxes are expected to be comparable even though the ^{40}Ca abundance typically exceeds that of ^{48}Ti in supernova ejecta (line saturation effect). The maximal model yields of ^{48}Ti in core-collapsed SNe range from about $4 \times 10^{-5} M_\odot$ (Woosley & Weaver 1995) to $2 \times 10^{-4} M_\odot$ (Thielemann et al. 1996), and are subject to rather substantial model uncertainties. Although core-collapsed SNe are naturally associated with molecular cloud environments (see e.g. Jiang et al. 2010) and reference therein, still SN Ia type origin can not be excluded for Kes 69, since no compact remnant has been found there yet. According to the models of SN Ia nucleosynthesis developed by Maeda et al. (2010), the yield of ^{48}Ti can exceed $10^{-3} M_\odot$ in SN Ia ejecta. Therefore, one may conclude that some ejecta fragments can show line emission of ^{48}Ti at the

⁵ As for the radio emission, the electrons accelerated at the fragment bow shock in most cases are in the MeV regime, well below GeV. So synchrotron radio emission is not expected to be observable for small fragments. However, an HII region may be created due to gas ionization by a powerful soft X-ray – far UV emission of the fragment bow shock. Bykov et al. (2008) made some simple modeling of the radio continuum from such an HII region that is expected to be produced by a fast ejecta fragment moving through dense ambient matter. The scale size of the radio emitting HII region is below arcmin if the distance to Kes 69 is about 5 kpc and its flux at 1.4 GHz is likely about 30 mJy (scaling from the IC443 case).

level estimated at 68% significance in Src 13 without any signs of ^{44}Ti , which is expected to decay at the estimated age of Kes 69. In conclusion, both the location, the X-ray spectra and the infrared counterpart of Src 3, 5, and 13 are consistent with the expectations for supernova ejecta fragments interacting with a dense ambient medium.

6.2. Alternative explanations

The X-ray spectra of Src 3,5 and 13 may also be fitted with a very hot thermal component. We have therefore explored other explanations for the detected sample of hard X-ray sources. Accreting dwarfs and stars with active coronae can be sources of hard X-ray emission (e.g. Fabian et al. 1976; Cordova et al. 1981; Patterson & Raymond 1985) and are therefore an interesting possibility. The X-ray luminosity of some CVs can reach up to $L_X \sim 10^{34}$ erg s $^{-1}$ (see e.g. Stacey et al. 2011), but the majority of CVs are much fainter. Integrated emission of CVs, especially of intermediate polars, is considered to be the dominating component in both the Galactic Center (see e.g. Munro et al. 2009) and Galactic Ridge emission (see e.g. Sazonov et al. 2006; Revnivtsev et al. 2009). Individual spectra of magnetic CVs, obtained with ASCA by Ezuka & Ishida (1999), show the Fe K_α emission lines, both the fluorescent emission at ~ 6.4 keV and from highly ionized Fe ions. The spectra can be attributed to the hot postshock plasma emission behind the accretion shock standing above the white dwarf surface. X-ray reflection from the white dwarf surface can account for the observed fluorescent Fe K_α line. Hard X-rays in the 17–60 keV band have been detected so far by *INTEGRAL* IBIS (see Lebrun et al. 2003; Ubertini et al. 2003) from 37 CVs (see, e.g., Krivonos et al. 2010). Thus, CVs could be alternative candidate sources for Src 3 and 5, but not for Src 13, due to the putative presence of Ca and ^{48}Ti lines along with the absence of Fe lines in its spectrum. However, while the ejecta shrapnel model can account for the emission in the 60 – 120 keV band with the flux of about 1.2×10^{-12} erg cm $^{-2}$ s $^{-1}$ detected by *INTEGRAL* ISGRI from Kes 69 field, the CVs most likely can not. Since the ejecta shrapnels are expected to be extended, dedicated *Chandra* observations can constrain the spatial extensions of Src 3, 5, and 13 to distinguish between the two interpretations.

7. Summary and conclusions

We have performed a study of the supernova remnant Kes 69 to search for compact hard X-ray sources. Such studies, carried out in remnants which are interacting with molecular clouds, may reveal a population of fast ejecta fragments, which may provide useful hints for the remnant progenitors. We have detected 18 sources in the 3–10 keV band, about 3 times the expected number of galactic sources in this area of the sky. Moreover, the position of the source are not random, but correlate with the CO emission of the cloud interacting with the remnant. We have selected 3 of the sources for further spectral analysis on the basis of the brightness and visual inspection of their spectra (Src 3, 5 and 13 in Table 1). The spectra can be fitted with a non-thermal model plus a few emission lines corresponding to K-shell transition of Si and Fe. We have also analyzed the Spitzer IRAC and MIPS image of the field, finding possible IR counterparts for Src 3, 5 and 13. The X-ray spectra and

IR flux ratio are consistent with a model of a fast ejecta fragment propagating inside the molecular cloud, making Kes 69 the second SNR for which an evidence exists for this new population of hard X-ray sources.

Uncertainties in the X-ray modeling makes the alternative explanation in terms of galactic cataclysmic variables also possible, but the excess with respect of $\log(N) - \log(S)$ counts, the location of the sources, the detection of the remnant by *INTEGRAL*/IBIS and some of the IR flux ratios make this interpretation less probable than the other. Further data are needed to say the final word about the nature of the sources.

Acknowledgements. This study has been supported by Ministry of Education and Science of Russian Federation (contract 11.G34.31.0001) and by the RFBR grants 11-02-12082-ofi-m-2011 and 11-02-00253. Support from P-21 and OFN-16 programs of RAS is acknowledged as well. AMK and YuAU acknowledge support from scientific school NSH-4035.2012.2. GGP acknowledges partial support from NASA grant NNX09AC84G. YC acknowledges support from the NSFC grant 10725312 and the 973 Program grant 2009CB824800. This work has been partially supported by ASI-INAF agreement n. 1/009/10/0.

References

- Abdo, A. A., Ackermann, M., Ajello, M., et al. 2010, *ApJ*, 712, 459
 Albert, J., Aliu, E., Anderhub, H., et al. 2007, *ApJ*, 664, L87
 Arnaud, M., Neumann, D. M., Aghanim, N., et al. 2001, *A&A*, 365, L80
 Aschenbach, B., Egger, R., & Trümper, J. 1995, *Nature*, 373, 587
 Bocchino, F. & Bykov, A. M. 2000, *A&A*, 362, L29
 Bocchino, F. & Bykov, A. M. 2003, *A&A*, 400, 203
 Bocchino, F., Krassilchtchikov, A. M., Kretschmar, P., et al. 2008, *Advances in Space Research*, 41, 396
 Bykov, A. M. 2002, *A&A*, 390, 327
 Bykov, A. M. 2003, *A&A*, 410, L5
 Bykov, A. M., Bocchino, F., & Pavlov, G. G. 2005, *ApJ*, 624, L41
 Bykov, A. M., Krassilchtchikov, A. M., Uvarov, Y. A., et al. 2008, *ApJ*, 676, 1050
 Condon, J. J., Cotton, W. D., Greisen, E. W., et al. 1998, *AJ*, 115, 1693
 Cordova, F. A., Mason, K. O., & Nelson, J. E. 1981, *ApJ*, 245, 609
 Dubus, G., Taam, R. E., Hull, C., Watson, D. M., & Mauerhan, J. C. 2007, *ApJ*, 663, 516
 Ezuka, H. & Ishida, M. 1999, *ApJS*, 120, 277
 Fabian, A. C., Pringle, J. E., & Rees, M. J. 1976, *MNRAS*, 175, 43
 Favata, F., Flaccomio, E., Reale, F., et al. 2005, *ApJS*, 160, 469
 Gezari, D. Y., Arendt, R. G., Smith, R., et al. 2006, *Journal of Physics Conference Series*, 54, 171
 Hands, A. D. P., Warwick, R. S., Watson, M. G., & Helfand, D. J. 2004, *MNRAS*, 351, 31
 Hewitt, J. W., Rho, J., Andersen, M., & Reach, W. T. 2009, *ApJ*, 694, 1266
 Jansen, F., Lumb, D., Altieri, B., et al. 2001, *A&A*, 365, L1
 Jiang, B., Chen, Y., Wang, J., et al. 2010, *ApJ*, 712, 1147
 Krivonos, R., Revnivtsev, M., Lutovinov, A., et al. 2007, *A&A*, 475, 775
 Krivonos, R., Tsygankov, S., Revnivtsev, M., et al. 2010, *A&A*, 523, A61
 Laming, J. M. & Hwang, U. 2003, *ApJ*, 597, 347
 Lebrun, F., Leray, J. P., Lavocat, P., et al. 2003, *A&A*, 411, L141
 Liedahl, D. A. 2005, in *American Institute of Physics Conference Series*, Vol. 774, X-ray Diagnostics of Astrophysical Plasmas: Theory, Experiment, and Observation, ed. R. Smith, 99–108
 Maeda, K., Röpke, F. K., Fink, M., et al. 2010, *ApJ*, 712, 624
 Makovoz, D., Roby, T., Khan, I., & Booth, H. 2006, in *Society of Photo-Optical Instrumentation Engineers (SPIE) Conference Series*, Vol. 6274, Society of Photo-Optical Instrumentation Engineers (SPIE) Conference Series
 Miyata, E., Tsunemi, H., Aschenbach, B., & Mori, K. 2001, *ApJ*, 559, L45
 Monet, D. G., Levine, S. E., Canzian, B., et al. 2003, *AJ*, 125, 984
 Motch, C., Warwick, R., Cropper, M. S., et al. 2010, *A&A*, 523, A92

- Muno, M. P., Bauer, F. E., Baganoff, F. K., et al. 2009, ApJS, 181, 110
- Nicastrro, F., Fiore, F., & Matt, G. 1999, ApJ, 517, 108
- Patterson, J. & Raymond, J. C. 1985, ApJ, 292, 535
- Reach, W. T., Rho, J., Tappe, A., et al. 2006, AJ, 131, 1479
- Revnivtsev, M., Sazonov, S., Churazov, E., et al. 2009, Nature, 458, 1142
- Sazonov, S., Revnivtsev, M., Gilfanov, M., Churazov, E., & Sunyaev, R. 2006, A&A, 450, 117
- Seward, F. D. 1990, ApJS, 73, 781
- Shaver, P. A. & Goss, W. M. 1970, Australian Journal of Physics Astrophysical Supplement, 14, 133
- Skrutskie, M. F., Cutri, R. M., Stiening, R., et al. 2006, AJ, 131, 1163
- Stacey, W. S., Heinke, C. O., Elsner, R. F., et al. 2011, ApJ, 732, 46
- Stolovy, S., Ramirez, S., Arendt, R. G., et al. 2006, Journal of Physics Conference Series, 54, 176
- Strüder, L., Briel, U., Dennerl, K., et al. 2001, A&A, 365, L18
- Thielemann, F.-K., Nomoto, K., & Hashimoto, M.-A. 1996, ApJ, 460, 408
- Tian, W. W. & Leahy, D. A. 2008, MNRAS, 391, L54
- Turner, M. J. L., Abbey, A., Arnaud, M., et al. 2001, A&A, 365, L27
- Ubertini, P., Lebrun, F., Di Cocco, G., et al. 2003, A&A, 411, L131
- Walter, R., Rohlfs, R., Meharga, M. T., et al. 2010, in Proceedings of the 8th INTEGRAL Workshop "The Restless Gamma-ray Universe" (INTEGRAL 2010). September 27-30 2010. Dublin Castle, Dublin, Ireland. Published online at <http://pos.sissa.it/cgi-bin/reader/conf.cgi?confid=115>
- Woosley, S. E. & Weaver, T. A. 1995, ApJS, 101, 181
- Yusef-Zadeh, F., Wardle, M., Rho, J., & Sakano, M. 2003, ApJ, 585, 319
- Zhou, X., Chen, Y., Su, Y., & Yang, J. 2009, ApJ, 691, 516

Appendix A: A simple method to assess the spatial correlation between a set of point-like source and the CO diffuse emission maps

Fig. 1, upper panel, shows the detected hard X-ray sources and the ^{12}CO contours emission in the 80-81 km s^{-1} range, which is the range of velocity associated with the Kes 69 remnant (Zhou et al. 2009). By eye, the source seem to be correlated with the cloud emission, but one need to assess this correlation in more detail. A simple way to do this is described below.

We have computed the histogram of the 80-81 km s^{-1} ^{12}CO brightness temperature map shown in Fig. 1, lower panel. This histogram is plotted as a solid line in Fig. 2 and has a peak around 2 – 2.5 K. We have also computed the brightness temperature at the locations of the 18 detected hard X-ray source in the same map, and we also computed the histogram and overplotted it as a dashed line in the Fig. 2. We stress that in case of a uniform distribution of the hard X-ray sources, their histogram should match the cloud histogram. If the sources tend to be located preferentially outside the cloud, the peak of their histogram should lie to the left of the peak of the cloud. Conversely, if the sources tend to be inside the cloud, their peak should fall at a temperature higher than the cloud temperature, which means that the source have a tendency to be located in regions of high brightness temperature. This is exactly what happens in case of the histograms computed using the 80 – 81 km s^{-1} ^{12}CO brightness temperature map (Fig. 2).

To further strengthen this argument, we have also computed the histogram using the 8-10, 50-60, 53-55 and 68-70 km s^{-1} ^{12}CO brightness temperature maps, using the data of Zhou et al. 2009, and we show them in Fig. A.1. These velocity ranges are not associated to the remnant and therefore they should be in foreground. Indeed, the plots show that the source histogram either has the peak at the same

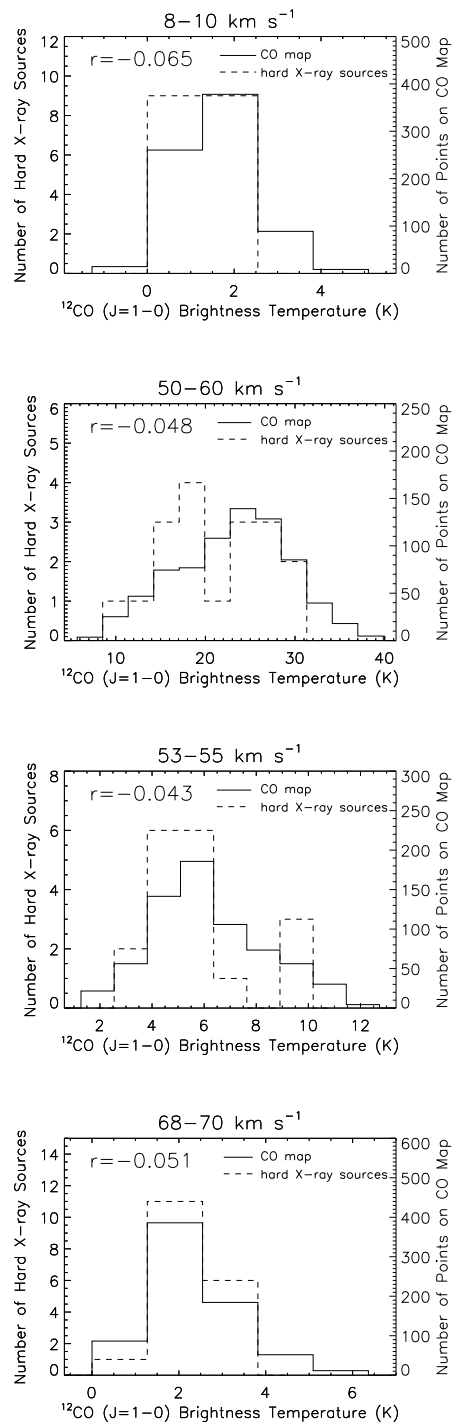


Fig. A.1. From top to bottom: as in Fig. 2 but for 8-10, 50-60, 53-55 and 68-70 km s^{-1} ^{12}CO brightness temperature maps

brightness temperature of the cloud histogram, or at lower brightness level, indicating little or negative correlation.

We have also calculated the Pearson's correlation coefficient r between the CO image and the hard X-ray sources image (an artificial image with the pixel values of one at the source position and zero elsewhere). This coefficient is 1 if the images are identical, > 0 if the two images are correlate, 0 if they are completely uncorrelated, and < 0 if they

are anti-correlated. The correlation coefficient r is shown in the upper-left corner of each image. The $80 - 81 \text{ km s}^{-1}$ histogram is the only one with positive r , i.e. the only one indicating a possible correlation between the sources and the ^{12}CO map.